Fire fragility curves for industrial steel pipe-racks integrating demand and capacity uncertainties

Abstract

This paper aims at deriving fire fragility curves for a prototype steel pipe-rack in an industrial plant subjected to localised fires. In particular, starting from a reference case study, uncertainties related to the structural capacity and the size of the localised fires caused by a hole in a tank or a hole in a pipe are included in the analyses. Thus, the influence of uncertainties in the derivation of the fragility functions was highlighted by comparing four sets of analyses in which both demand and capacity uncertainties were progressively introduced. Moreover, alongside the cloud analysis (CA), the suitability of the Multiple Stripe Analysis (MSA) to build relevant probabilistic fire demand models was assessed. Fire fragility curves were derived by considering the interstorey drift ratio (ISDR) as engineering demand parameter (EDP) and by assessing different relevant intensity measures (IMs) that represent the severity of localised fires. It was found that by introducing uncertainties in the steel yield strength, lower probabilities to exceed the life safety and the near collapse limit states with respect to the reference case study were observed. Moreover, the inclusion of further uncertainties, described with continuous physically-based probability functions of the size of the fire diameter, affected the probabilistic models by lowering the probability of exceedance. These functions provide a more realistic description of the fire scenario, enabling a better representation of the structural vulnerability. For this case study, the CA exhibited better suitability for the derivation of fire fragility curves than the MSA. All the analysis results are thoroughly discussed in the paper.

Keywords

Parameter uncertainties; Cloud analysis; Multiple Stripe analysis; Localised fires; Probabilistic fire demand model; Steel pipe-rack structure

1. Introduction

Fire safety is a fundamental requirement of the design of civil and industrial structures, which according to the current European norms [1] may be satisfied by employing either a prescriptive or a performance-based approach. The prescriptive approach mainly consists in "deemed-to-satisfy" solutions and employs nominal fire curves, e.g., ISO 834 or hydrocarbon curves, that do not represent the real fire behaviour. Instead, Performance-Based Fire Engineering (PBFE) provides performance objectives and requirements to be satisfied and exploits more realistic fire curves, that consider the fire characteristics and the environment in which the structure is located. In general, PBFE allows for a better description of the actual fire behaviour, an increase in design flexibility and a reduction of the construction costs but, on the other hand, it entails an adequate expertise of the designer and the employment of advanced tools, like numerical software for thermal and structural analyses or probabilistic frameworks for the definition of plausible fire events or for fire risk assessment. Whilst numerical simulation of several types of structures and resisting mechanisms in fire can rely on thoroughly validated software and new developments, suited for the investigation of complex phenomena [2-8], the extension of probabilistic concepts to fire safety engineering requires separate studies addressing specific structural types, fire characteristics and scenarios. In this respect, fragility functions/curves are useful tools for risk assessment, hazard mitigation and expected damage estimation of structures and infrastructures, but their implementation in fire engineering is still at an initial stage, in particular for industrial plants. As performance-based fire engineering and fully probabilistic structural fire engineering approaches are arising in the design practice, the definition of probabilistic fire demand models (PFDMs) and fire fragility curves is becoming important. Indeed, despite meaningful indications of different nature can be obtained by applying the PBFE with a deterministic approach [9-14], a probabilistic approach provides more general considerations, as well as useful tools, like fire fragility curves, which show the probability of exceedance of specific limit states, defined according to appropriate engineering demand parameters (EDP), conditioned on a suitable intensity measure (IM) that characterise the fire, such as the fire dimension or the fire load.

These curves may be integrated in a fully probabilistic structural fire engineering (PSFE) framework, contributing, for instance, to estimate the expected damage of a structure when combined with probabilities of occurrence of fires in a specific context, e.g. residential or industrial.

Though the probabilistic approach has been widely exploited in Performance-Based Earthquake Engineering (PBEE) [15-20], there are only a few works focused on the development of fire fragility curves [21-25]. Among the others, in [22, 23] a methodology for developing fire fragility curves for steel structures exposed to compartment fires, relevant to office and dwelling buildings, was presented. Lange et al. [24] and Shrivastava et al. [25] adapted the probabilistic framework of the Pacific Earthquake Engineering Research Center (PEER) [26] to fire engineering. In addition, methods to compute fragility curves were mainly deployed in the context of PBEE. For instance, the three main methods used to build probabilistic demand models: cloud analysis (CA), incremental dynamic analysis (IDA), and multiple stripe analysis (MSA), were compared in [15]. Shome et al. [16] and Cornell et al. [17] laid the groundwork for the adoption of cloud analysis in seismic applications. Baker [18] instead, investigated incremental dynamic analysis and multiple stripe analysis and developed a fragility functions fitting based on a maximum likelihood estimation. Luco and Cornell [19] described the concepts of efficiency and sufficiency of an IM to assess its suitability for developing seismic fragility functions, while a relative measure between two IMs, i.e., relative sufficiency, was proposed as alternative sufficiency indicator in [20].

Probabilistic fire analyses and fragility curves become even more rare when it comes to industrial and petrochemical plants, though their piping systems mainly transport flammable material, liquid or gas fuel. Natural or accidental events may severely damage the structure supporting the piping systems [27-32], usually consisting of steel pipe-racks, and they may cause a release of flammable material from a pipe or a tank. Although in general the probability of occurrence of a fire may be low, the probability of ignition of the spilled flammable material increases in industrial environments and severe consequences are expected, as shown, among the others, by Uehara [33], Chan and Lin [34], Zheng and Chen [35] and Shu and Chong [36]. Therefore, the fire risk cannot be ignored for

petrochemical plants, and the definition of specific probabilistic fire demand models (PFDMs) is desirable. For this purpose, plausible fire scenarios, representing pool fires resulting from leakage and loss of containment from a pipe or a tank, should be defined. Methods to quantify the probability of occurrence of a loss of fuel and the characteristics of the arising fires, e.g., the mass flow rate resulting from a fuel leakage through a hole in a tank or in a pipe, were provided in [37-40]. These methods introduce a variability in the fire characteristic, or in general in the fire demand, that should be carefully considered when developing PFDMs. However, uncertainties may affect the capacity of the structures as well. In this respect, Gernay et al. [22, 23] indicated several sources of uncertainties that may influence the structural capacity of residential or office buildings, like the randomness in the material properties and in the magnitude of the loads. Recently, a probabilistic model for the steel properties at elevated temperature was illustrated in [41, 42].

In this context, this paper gives a novel contribution to the field by developing fire fragility curves for a prototype steel pipe rack exposed to localised fires, considering both demand and capacity uncertainties, that will be useful to apply in probabilistic frameworks to estimate the expected damage and/or in fire risk assessment analyses. It investigates the effect of including different uncertainties by increasing the number of uncertain parameters and finally provides fragility curves that are representative of a more realistic description of the fire scenario and structural behaviour. In detail, starting from a reference case study presented in [43], additional numerical analyses were performed, first integrating randomness in the steel material properties at elevated temperature, and then introducing variability of fire characteristics for both material loss from a hole in a tank or in a pipe in the model. To evaluate the effects of demand and capacity uncertainties, the four different sets of analyses were compared throughout the whole procedure that brought to the development of fire fragility curves for three relevant IMs. Among the different IM, a scaled distance, based on concepts employed to describe blast or explosion hazard and obtained as a simple function of the fire parameters, is proposed to characterise the fire severity. Efficiency and relative sufficiency concepts were used to determine the most suitable IMs and the employment of not only the CA but also of the

MSA for building the fragility curves was investigated. The numerical analyses were carried out with the software SAFIR [2], since it enables both structural and thermal analyses, and includes the LOCAFI model for localised fires. Indeed, numerous works have investigated the thermal radiation emitted from hydrocarbon pool fires to propose fire models [44-50], but only recently an analytical model for localised fire, namely LOCAFI, was developed and integrated in a software [51-55]. This model quantifies the thermal impact of localised fires on vertical structural elements assuming that the flame shape is conical and based on the Heskestad flame length and temperature correlations [46, 55].

The paper is organised as follows: in Section 2 the prototype steel pipe-rack is described along with the fire scenarios and the uncertain parameters; Section 3 presents the probabilistic fire analysis and the derivation of the fire fragility curves; finally, in Section 4 the conclusions and the future perspectives are drawn.

2. Description of a prototype steel pipe-rack subjected to localised fires

In this section the prototype steel pipe-rack is presented, together with its numerical modelling. Analogously, the pool fire scenarios and the associated localised fire models are described as well. Finally, the probabilistic approach employed to account for uncertainties is outlined and the structure of the numerical analyses is delineated. For comparison purposes, four case studies are defined depending on the source of the uncertainties introduced in numerical simulation. Further details on the structural and fire models adopted in the analyses can be found in [43].

The case study is based on an existing petrochemical plant located in Italy, whose seismic behaviour was thoroughly studied [28-31], and it is composed of several steel frames with rigid beam-to-column joints, pinned column-base joints in the transversal direction and vertical braces in the longitudinal direction with repeated modules composed of seven bays and only one equipped with bracings. The structural contribution of the piping system was neglected, and the geometry of the supporting steel pipe rack was simplified, resulting in the case study depicted in Figure 1. A regular portion of the structure was analysed, consisting of a six-bay module frame with a total extension of L_s=36m. The

vertical load due to the self-weight of the pipes and their content was assumed equal to q_V=75kN/m, whilst a horizontal load q_H=2kN/m was applied to take into account the friction of the pipes. Moreover, point loads were applied at midspan of the longitudinal beams, i.e., V=15kN vertical and H=7.5kN horizontal loads. As for the fire models later described in this paper, wind effects were neglected and no wind loads were applied.

The numerical model was defined with the thermo-mechanical non-linear finite element software SAFIR [2]. In detail, the model comprised HEA 340 columns, HEA 200 longitudinal beams, a lower row of HEA 300 transversal beams and HEB 300 for the remaining transversal beams, all made of S275 steel. 936 3D Bernoulli beam finite elements, having length of 50 cm each, were employed in the analyses. Columns were pinned at their base in both principal directions, transversal beams were end fixed to the columns, whilst the longitudinal beams were pinned to the columns (Figure 1b). Since the heating of the longitudinal bracing system, based on the investigated fire scenarios, was very limited and the major thermal impact occurred in the transverse direction, the bracing system was substituted in the model with horizontal restraints in the longitudinal direction to limit the computational burden.

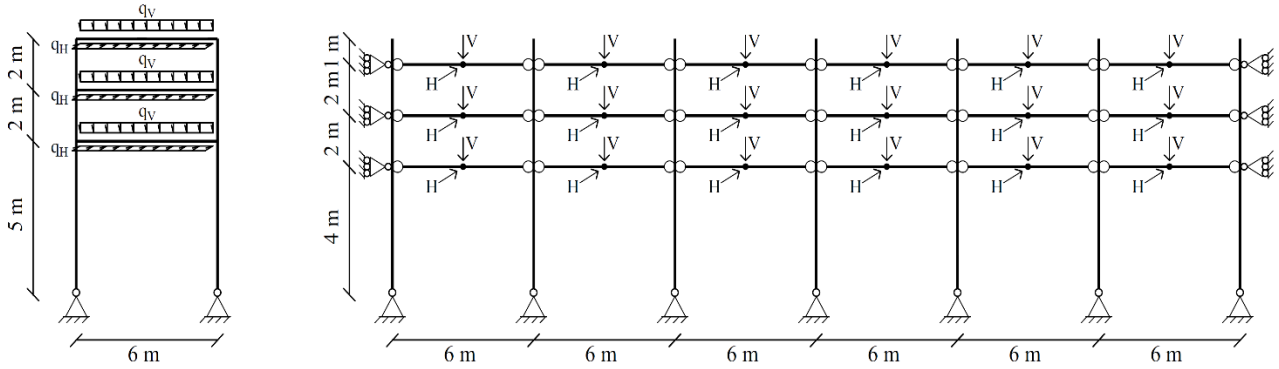

Figure 1. Case study

2.1. Fire scenarios description and localised fire models

Fire scenarios consisting of pool fires resulting from a flammable material leakage or from a burning tank (Figure 2a) in industrial plants were investigated. A meaningful set of plausible localised fires impacting the structure with different levels of intensity, that cause from low consequences to the collapse of the entire structure, was considered. The set of scenarios was defined varying three

parameters, i.e., the fuel type, the fire diameter D and the fire-structure distance d, where the latter is the distance separating the edge of the fire and the structure. As shown in Figure 2b, the fires were always located in front of the structure, with the fire centre aligned with the central transversal beam of the structure. The distance between the fire centre and the structure is indicated as L. The analyses performed in [43], used as reference in this work and referred to as Case Study 0 (CS0), were performed employing the pool fire parameters reported in Table 1. Such analyses were expanded in this work as described in Section 2.2.

Table 1. Set of pool fire scenarios – fuel, fire-structure distance d and fire diameter D values used in the reference analysis - CS0

Pool fire parameters		Number of analyses
Fuels	Pentane, Kerosene, Heptane, Gasoline, Fuel Oil, Benzene, Acetone	7
Distance d [m]	0.5, 1, 2, 3, 4, 5, 6	7
Diameter D [m]	5, 7.5, 10, 12.5, 15, 17.5, 20, 22.5, 25, 27.5, 30	11
Total number of analyses		539

In CS0 7 liquid fuels were selected for the definition of the fire scenarios, since petrochemical plants deal with various flammable products, as well as 7 fire-structure distances. Distances higher than 6 m were not investigated since for d=6 m the selected fires were already having a limited impact on the structure. Eleven equally spaced diameters were considered, assuming a uniform distribution of diameters in the 5 m to 30 m range, i.e., fires with diameters in the selected range all occur with the same probability, without distinguishing between leakage from a hole in the tank or from a pipe (Figure 2a). By varying the three parameters, 539 different localised fires were obtained and for each of them a thermo-mechanical analysis was performed, considering 60 minutes of thermal exposure.

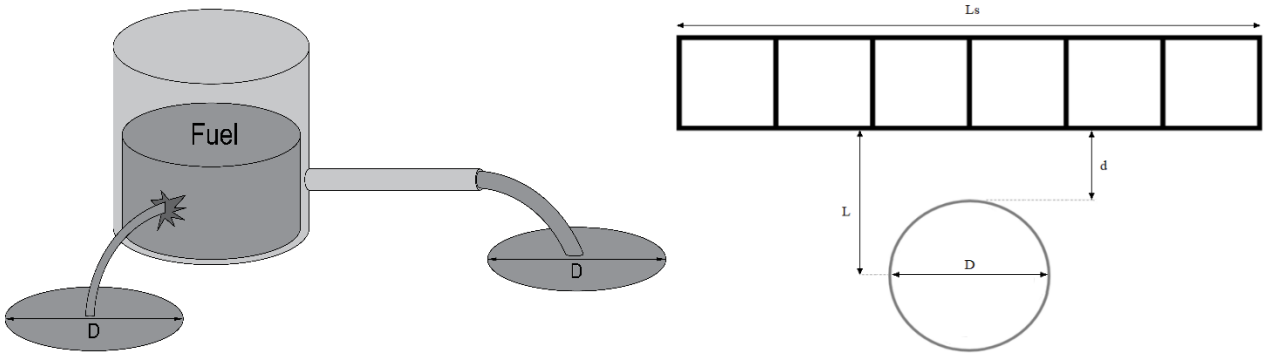

Figure 2. a) Liquid outflow through a tank or a pipe; b) Fire-structure distance d and fire diameter D

A localised fire model integrated in SAFIR was employed to describe the fire development. Such model, i.e, LOCAFI model [55], belongs to the category of analytical models that exploit the virtual solid flame concept and was proven to provide accurate results, without being as demanding as more refined computational fluid dynamics (CFD) models. The model relies on the existing Heskestad correlations for localised fires included in Annex C of EN1991-2 [1] and describes a localised fire with a conical shape. It was validated against experimental data of fires characterised by diameters up to 50 m [55,56]. Localised fires are obtained in the model by defining the fire diameter D and the rate of heat release (RHR) Q of the fire. Indeed, additional information as the flame length L_f and temperature evolution along the flame axis can be derived from these two parameters

$$\begin{aligned} L_f &= 0.0148Q^{0.40} - 1.02D \text{ [m]} \\ T(z) &= 20 + 0.25Q_c^{\frac{2}{3}}(z - z_0)^{-\frac{5}{3}} \leq 900 \text{ [°C]} \end{aligned} \quad (1)$$

with

$$Q_c = 0.8Q \text{ [W]} \text{ and } z_0 = 0.00524Q^{0.40} - 1.02D \text{ [m]} \quad (2)$$

Where Q_c is the convective part of the rate of heat release Q and z_0 is the virtual origin of the fire source. The rate of heat release Q employed in the analyses was obtained as follows

$$\begin{aligned} Q &= \dot{m}_b \Delta H_c \left(\frac{D\pi^2}{4}\right) \text{ [kW]} \\ \dot{m}_b &= \dot{m}_\infty \left(1 - e^{-k\beta D}\right) \left[\frac{kg}{m^2 s}\right] \end{aligned} \quad (3)$$

where the mass burning rate $\dot{m}_b$ was defined by Zabetakis and Burgess [58]. $\dot{m}_\infty$ is the limiting mass burning rate, kβ is the empirical constant defined as the product between the extinction coefficient k and the mean beam length corrector β and ΔH_c is the heat of combustion (kJ/kg). The values employed in the analyses are reported in Table 2 [59]. For pentane the mass burning rate was taken as the limiting mass burning rate, and thus, no empirical constant is provided in Table 2. As a reference value to quantify the fuel intensity, the equivalent RHR density of the fuel q was obtained as follows

$$q = Q/\left(\frac{D\pi^2}{4}\right)\ [MW/m^2],\ \text{with } \dot{m}_b = \dot{m}_\infty \quad (4)$$

Table 2. Fuel properties

Fuel	Limiting mass burning rate $\dot{m}_\infty$ [kg/m²s]	Empirical constant $k\beta$ [m⁻¹]	Heat of combustion ΔH_c [kJ/kg]	Equivalent RHR density q [MW/m²]
Acetone	0.038	2.24	25800	0.98
Fuel Oil	0.034	1.67	39700	1.35
Gasoline	0.055	1.48	43700	2.40
Kerosene	0.063	1.27	43000	2.71
Benzene	0.085	2.70	40100	3.41
Heptane	0.081	1.39	44600	3.61
Pentane	0.095	–	48800	4.64

2.2. Uncertainties in the structural and in the fire models

In CS0 [43] the variability of the fire input, or in general of the thermal demand, was accounted for by varying the parameters characterising the fire considering a predetermined set of values. However, a probabilistic approach, accounting also for uncertainties that may have a significant impact on the structural capacity, e.g., steel mechanical and thermal properties and the applied loads [22], should be preferred. In the specific case of the analysed pipe-rack, applied vertical loads are well defined in case of normal service conditions, meaning that no significant variation is foreseen. Conversely, the uncertainty related to the steel properties, and in particular to the mechanical properties, may significantly affect the structural behaviour, as highlighted in [22,23]. Nevertheless, steel thermal properties have relatively low variances and the deterministic values from EN-1993-1-2 [57] can be taken [22]. Based on this discussion, in this work a probabilistic approach was adopted to consider uncertainties affecting both the fire demand and the structural capacity with reference to the yield strength at ambient and at elevated temperature. Starting from the reference case study CS0, uncertainties related to the steel yield strength were implemented in a new set of analyses, namely Case Study 1 (CS1). In detail, in CS0 the properties of steel at elevated temperature were taken as in EN 1993-1-2 [57], whilst the analyses summarised in Table 1 were run in CS1 by considering the logistic EC3-based probabilistic model proposed by Khorasani et al. [41] and Qureshi and al. [42] for the yield strength at elevated temperature, whereas the Young's modulus and the proportional limit

were taken as in EN 1993-1-2 [57]. In this model the reduction of the yield strength at elevated temperature follows a probabilistic distribution, in which the variability of the value of the retention factor k_y, defined as the yield strength at a given temperature T measured at a 2% strain normalized by the yield strength at room temperature, is accounted for by means of the following equation

$$k_y = \frac{1.7 \exp\left[\text{logit}\left(\hat{k}^*{}_y\right) + 0.412 - 0.81 \cdot 10^{-3} \cdot T + 0.58 \cdot 10^{-6} \cdot T^{1.9} + 0.43\varepsilon\right]}{\exp\left[\text{logit}\left(\hat{k}^*{}_y\right) + 0.412 - 0.81 \cdot 10^{-3} \cdot T + 0.58 \cdot 10^{-6} \cdot T^{1.9} + 0.43\varepsilon\right] + 1} \quad (5)$$

where

$$\text{logit}\left(\hat{k}^*{}_y\right) = \ln\left(\frac{\hat{k}^*{}_y}{1-k^*{}_y}\right), \hat{k}^*{}_y = \frac{k_{y,EN1993-1-2}+10^{-6}}{1.7} \quad (6)$$

$k_{y,EN1993-1-2}$=$k_{y,EN1993-1-2}(T)$ is the retention factor of the yield strength at elevated temperature according to EN1993-1-2 [57] and ε is the standard normal distribution. The yield strength at ambient temperature also varies according to Eqs. (5) and (6) in terms of ε. Hence, the change in the steel strength with temperature was characterised by a different k_y reduction factor, determined according to Eq.(5) and values of ε generated with a Latin Hypercube sampling, in each one of the 539 analyses. Figure 3a illustrates the distributions of the retention factors k_y obtained at different temperatures, i.e. 20°C, 400°C and 600°C. It can be observed that the probabilistic model allows for higher retention factors and in turn yield strengths, compared to the EN1993-1-2 until very high temperatures are reached. In detail, the 0.5 quantile of k_y is always higher than $k_{y,EN1993-1-2}$ for T<700°C, whilst the mean of k_y is higher than $k_{y,EN1993-1-2}$ until approximately 900°C. In particular, as reported in [60] the logistic model described in Eqs. (5) and (6) implicitly includes the effect of strain hardening at lower temperatures and therefore, k_y can be higher than 1.0 at ambient temperature and consequently higher than $k_{y,EN1993-1-2}$. In this respect, the characteristic yield strength value was used in order to avoid too large yield strength values at ambient temperature.

Two further set of analyses, namely Case Study 2 (CS2) and Case Study 3 (CS3), were carried out to propose a more refined thermal demand model for which the fire diameter was computed with continuous physically-based probability distributions based on the leakage of flammable material

226 from a hole in the tank or from a pipe. Indeed, in [43] the two probability density distributions were
227 obtained by quantifying the liquid flow from a tank through a hole, or a pipe respectively. They were
228 derived in order to determine the dimension of the fires that were most likely to occur and to be
229 enough severe for the structure. For each of the two scenarios, consisting of 1000 different
230 configurations, the fuels reported in Table 1 were considered and random tank and pipe geometries,
231 hole dimensions and tank filling degrees varying within realistic ranges were selected. These analyses
232 resulted in the fire diameter distributions depicted in Figure 3b. The illustrated normal distributions
233 are defined with a mean of 20.39 m and a standard deviation of 14.75 m for a fuel leakage through a
234 pipe and with a mean of 17.93 m and a standard deviation of 13.11 m for a fuel leakage through a
235 hole. Therefore, the analyses of CS2 and CS3 were performed considering the diameter distributions
236 for a liquid outflow from a pipe and from a hole, respectively. For each of the 49 fuel-distance pairs,
237 11 diameters D were used from a set of 539 values picked with a Latin Hypercube sampling from the
238 distributions. In Figure 3b also the distribution of the set of diameters employed in CS0 and CS1 is
239 reported for comparison purposes. A summary of the quantities differentiating the 4 sets of analyses
240 is provided in Table 3.

241 **Table 3.** Features of the investigated sets of analysis

Sets of analysis	Demand parameters	Capacity parameters
	Diameter D [m]	**Steel yield strength**
CS0	Uniform distribution (Table 1 & Figure 3b)	Deterministic (EN 1993-1-2 [57])
CS1	Uniform distribution (Table 1 & Figure 3b)	Probabilistic (Eq. 1)
CS2	Probabilistic (Figure 3b – pipe)	Probabilistic (Eq. 1)
CS3	Probabilistic (Figure 3b – hole)	Probabilistic (Eq. 1)

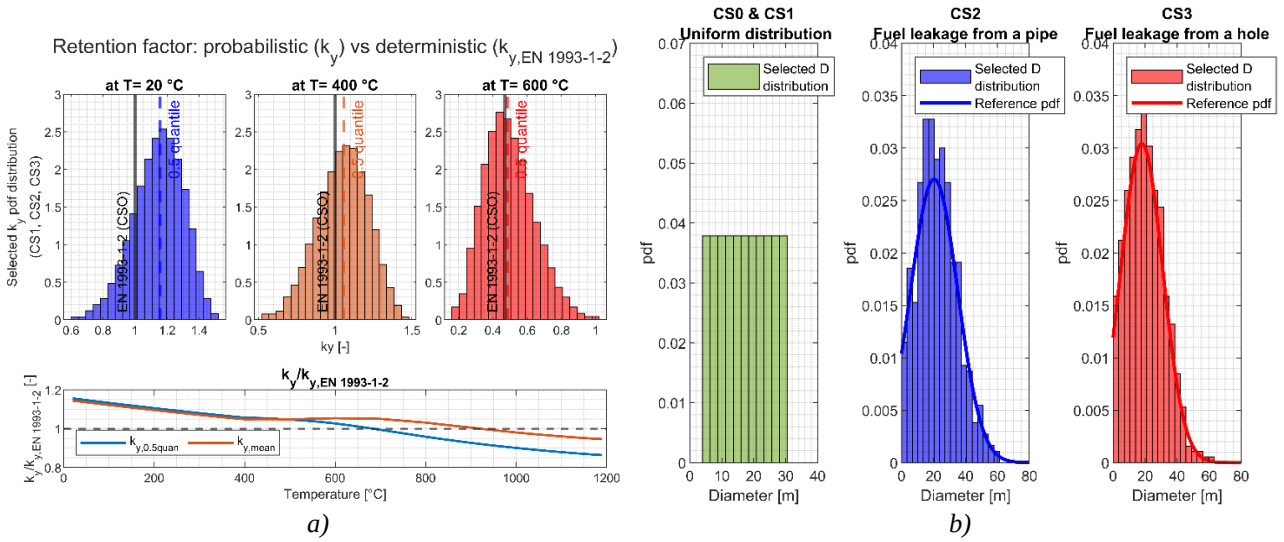

a) *b)*

Figure 3. a) Probabilistic (Qureshi and al. [42]) vs deterministic retention factor model; b) Diameters distributions in CS0&CS1, CS2 and CS3

3. Probabilistic fire analysis

In this work, the results of numerical analyses are used to define a probabilistic fire demand model, with the aim to develop fire fragility curves, by providing a useful tool for practitioners that want to probabilistically assess or design a steel pipe-rack structure subjected to localised fires. Such curves describe the probability that an engineering demand parameter (EDP) exceeds a structural limit state (LS) conditioned on an intensity measure (IM).

$$P(EDP > LS|IM) \tag{7}$$

It is evident, that the selection of appropriate engineering demand parameters (EDP) and intensity measures (IMs) is crucial to propose fire fragility curves that accurately describe the structural response and the severity of the action. In this context, a significant data elaboration process had to be performed in order to only present the outcomes that provide a valuable information in terms of the selected EDPs and IMs. Therefore, in Section 3.1 and 3.2 suitable relevant IMs and EDPs are described.

3.1. Intensity measures

A good IM for a PFDM should be able to properly represent the severity of the fire scenario. In the literature several IMs have been proposed for compartment fires, but their ability to characterise

localised fires is not guaranteed. Therefore, the 8 IMs reported in Table 4 are investigated. The first 7 were proposed by Randaxhe et al. [43], whereas the last one has been added in this work. Three obvious choices for the IMs consisted in the 3 parameters characterising the fire scenarios, i.e., the fire diameter D, the structure-fire distance d and the equivalent RHR density q. The latter is obtained assuming that $\dot{m}_\infty = \dot{m}_b$, which is a good approximation for D > 1 m. The remaining IMs were selected as functions of D, d and q. The fire position-diameter ratio was computed by considering the distance between the structure and the fire centre L as D/2+d. Instead, Eq.(1) was employed in the definition of the flame length L_f and the structure fire distance-flame length ratio d/L_f. HF_{avg} was obtained by means of a weighted average of the heat fluxes HF on the four sides of the cross section when it was impinged by the maximum radiative heat flux obtained with the LOCAFI model [55].

The RHR density q is typically employed as IM in applications for compartment fires [22-25], since it provides an accurate estimate of the fire severity when a uniform fire distribution is assumed in an entire compartment. However, the RHR density q cannot accurately describe the severity of fires developing in a limited zone that might be far from the structure, i.e. localised fires. In particular, the fire dimensions and the distance separating the structure and the fire might influence the heat flux received from the structure and the number of critical elements that are severely heated.

In order to provide an indicator that considers these aspects and more accurately characterises the severity of a localised fire, a further IM was defined, namely the scaled distance $d/A_{b,PE,eq}$ (Table 4). As shown later in this paper, the scaled distance is one of the best IM candidates yet being much simpler to derive than HF_{avg} and is obtained as the ratio between the structure-fire distance d and the equivalent pentane surface $A_{b,PE,eq}$, computed as

$$A_{PE,eq} = \frac{Q}{\dot{m}_{b,PE}\Delta H_{c,PE}} = \frac{q\left(1 - e^{-k\beta D}\right)\left(\frac{\pi D^2}{4}\right)}{\dot{m}_{b,PE}\,\Delta H_{c,PE}} \ [m^2] \quad (8)$$

Where $\dot{m}_{b,PE}$ and $\Delta H_{c,PE}$ are the mass burning rate and the heat of combustion of pentane, respectively (Table 2). $A_{b,PE,eq}$ represents the equivalent surface of pentane to obtain the same RHR of the actual localised fire. Thus, the lower the scaled distance $d/A_{b,PE,eq}$ the higher the severity of the fire. It is

worth to point out that in the development of fragility curves related to the blast or explosion hazard, a scaled distance is widely employed as IM, e.g. in [61-63], which is defined as the structure-explosion distance over a fractional power of an equivalent TNT mass M_{TNT}. Analogously to $A_{b,PE,eq}$ (Eq. (8)), M_{TNT} is obtained as the mass of TNT that is necessary to obtain the same energy released by the actual explosion.

Table 4. Investigated Intensity Measures (IM)

IM	Name	Function/Formula
D [m]	Fire diameter	$f(D)$
d [m]	Structure fire distance	$f(d)$
q [MW/m^2]	Equivalent RHR density of the fuel	$f(q) = \dot{m}_{\infty}\Delta H_c$
L/D	Fire position-Diameter ratio	$f(D,d) = (D/2 + d)/D$
L_f [m]	Flame length	$f(D,q) = \text{Eq.}(1)$
HF_{avg} [kW/m^2]	Maximum average heat flux impinging the structure	$f(D,d,q)$ see [26]
d/L_f	Structure fire distance-Flame length ratio	$f(D,d,q) = d/\text{Eq.}(1)$
$d/A_{b,PE,eq}$ [m^{-1}]	Scaled distance	$f(D,d,q) = d/\text{Eq.}(8)$

3.2. Engineering demand parameters

The EDP should be a good indicator of the structural response, but an EDP suited for a particular case might not be the best choice for a different structure or for a different action (e.g., fire, seismic, impact, etc.). For instance, the maximum temperature and the vertical deflections of the structural members may be identified as relevant EDPs for steel buildings exposed to compartment fires but are not suited for the proposed case study. Indeed, since the structural members are not engulfed in fire, limited vertical deflections were registered and a single temperature measure cannot adequately represent the complex thermal distribution inside and along the structural members. Therefore, in [43] the numerical results were examined thoroughly to identify an adequate EDP among different candidates, e.g., the inter-storey drift ratio, the axial load and the bending moment in the structural elements, the maximum average temperature within the whole structure and the average temperature within the most stressed structural elements. Finally, the inter-storey drift ratio (ISDR) was selected as EDP since it accurately represents the structural state regardless from the fire scenario and is widely employed for other types of structures and actions, e.g., seismic actions. Indeed, despite in general

thermally induced drifts are not directly correlated to damage, in the investigated case study large drifts were the major contributing cause of structural failure. Moreover, though localised fires may induce differential ISDR at the same floor, numerical results showed that in this work the ISDR could be associated with the damage of a significant part of the structure and thus, could be taken as an indicator of the global structural response.

Detailed information on the values of ISDR associated to specific structural damage states (LS in Eq. (7)) is available in literature. In this study, the ISDR values of 5% and 2.5% were adopted for near collapse limit state and life safety limit state respectively, according to the indications for steel moment resisting frames of the American seismic rehabilitation prestandard [64]. The selected limit states refer to a situation in which a small increase of thermal and/or mechanical loads would lead the structure to failure, i.e. near collapse, or to a situation in which the structure is in a significant deformative state, but still has a margin of bearing capacity to support additional thermal and/or mechanical loads, i.e., life safety.

3.3. Results of the numerical analyses

The results of the 2156 numerical analyses performed for the four case studies (i.e., 4 x 539 analyses) are reported. If failure was not attained earlier, the analyses were stopped at 60 min, since by preliminary checks it was found that thermal equilibrium was reached in the steel members after that time. Figure 4a and Figure 4c show the typical deformed shape of the structure at failure and after 60 minutes, respectively. Figure 4 refers to CS3 and Figure 4a and Figure 4b depict the structure exposed to a heptane fire at a distance of 2 m and a diameter of 25.4 m, whereas Figure 4c and Figure 4d show the case with a heptane fire but diameter equal to 11.0 m. As depicted, the typical failure mechanism of the structure consisted in the loss of stability of the central frame, which in most of the cases experienced the largest transversal deformations. Despite the maximum displacements occurred at the top of the structure, the highest inter-storey drift ratios (ISDR) were registered in the transverse direction at the first level of the columns, i.e, at a height of 5m. Since no load increments were applied,

the progressive increase of the transversal displacements was related to the effects of the fire exposure. Indeed, strength and stiffness degradation of steel occurred and consequently the load-bearing capacity of the structural members decreased. In addition, the structural members were partially restrained; thus, axial dilatation and thermal bowing of the members induced variations of the internal forces. In particular, thermal bowing in the columns was substantial due to the significant non-uniform temperature distributions in the cross sections and entailed an increase in second order effect importance, as depicted in Figure 4b and Figure 4d for the central column of the closest row to fire at a height of 5m.

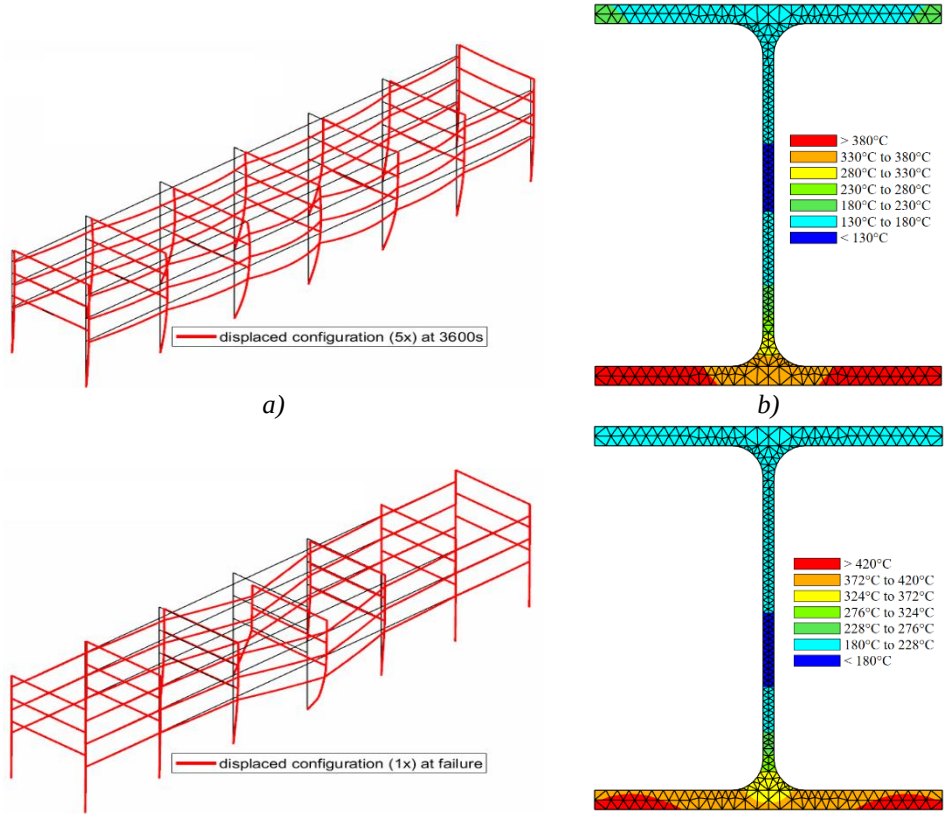

a) *b)* *c)* *d)*

Figure 4. CS3 – Fuel=Heptane, d=2m: a) D=25.4m, deformed shape at failure; b) D=25.4m, temperatures of the front row central column at 5m at failure; c) D=11.0m, deformed shape after 60 minutes; d) D=11.0m, temperatures of the front row central column at 5m after 60 minutes

The maximum inter-storey drifts obtained in the analyses are represented in Figure 5 and Figure 6 and they are denoted as ISDR for CS0, and as ISDR(ε) for CS1-CS3, where the steel yield strength at elevated temperature varied in accordance with the standard normal distribution ε in Eq.(5). The regions relevant to the life safety limit state and the near collapse limit states are indicated in green (2.5%≤ISDR<5%) and in red (ISDR≥5%).

345 The effects of the introduction of the variability in the steel material properties can be discussed
346 observing the comparison between ISDR from CS0 and CS1 proposed in Figure 5a. A good
347 correlation is found between the results of the two analyses (mean and standard deviation of the ISDR
348 are 0.96% and 0.09% respectively), but accounting for the steel yield strength uncertainties tends to
349 reduce the ISDR in CS1. The points inside the green and red shaded areas represent the analyses
350 exceeding both the life safety and the near collapse limit state for each single analysis of the two sets,
351 i.e. CS0 and CS1. Instead, the points lying inside the blue areas are associated with the analyses for
352 which the near collapse limit state was exceeded in one CS, but only the life safety limit state was
353 reached for the other CS. In this respect, the CS0 deterministic material property assumptions appear
354 more severe since analyses that exceed the near collapse for CS0 are, conversely, in many cases still
355 only exceeding the life safety limit state for CS1. Indeed, in CS1 the steel retention factors of the
356 yield strength are on average larger than the one prescribed in the EN 1993-1-2 and used in CS0 (see
357 the 0.5 quantile and the mean of the picked k_y factors in Figure 3). Thus, higher strength is exhibited
358 in the CS1 analyses. This holds true when the ISDR of CS0 are compared to the ones of CS2 and CS3
359 as also in these cases the probabilistic material model was considered, as shown in Figure 5b. In
360 addition, the mean ISDRs of CS1, CS2 and CS3, i.e., 3.59%, 3.67%, 3.60%, reflect the mean of the
361 diameter distributions employed in such analyses, i.e., 17.5m, 20.39m, 17.93m. Larger diameters
362 entail more severe fires, leading to higher values of ISDR.
363 To better understand the effects of uncertainties, the results of each of the analyses performed for
364 CS2 and CS3 were examined. As mentioned before, since the LOCAFI model was not extensively
365 investigated for fire diameters larger than 50 m (D>50 m) [55,56], the analyses obtained for diameters
366 larger than 50 m in CS2 (14 analyses) and in CS3 (5 analyses) are explicitly indicated in Figure 5b
367 with grey squares and are not considered later in the development of the PFDMs. Besides, it has to
368 be observed that some analyses experienced ISDR>5% without showing structural failure owing to
369 lack of numerical convergence caused mainly by material fracture occurred in a highly deformed
370 configuration, that also determined runaway in some analyses. Therefore, the analyses run until the

end (60 minutes). For such analyses it was checked that by slightly increasing the loads, failure was reached to confirm that they were in a near collapse state.

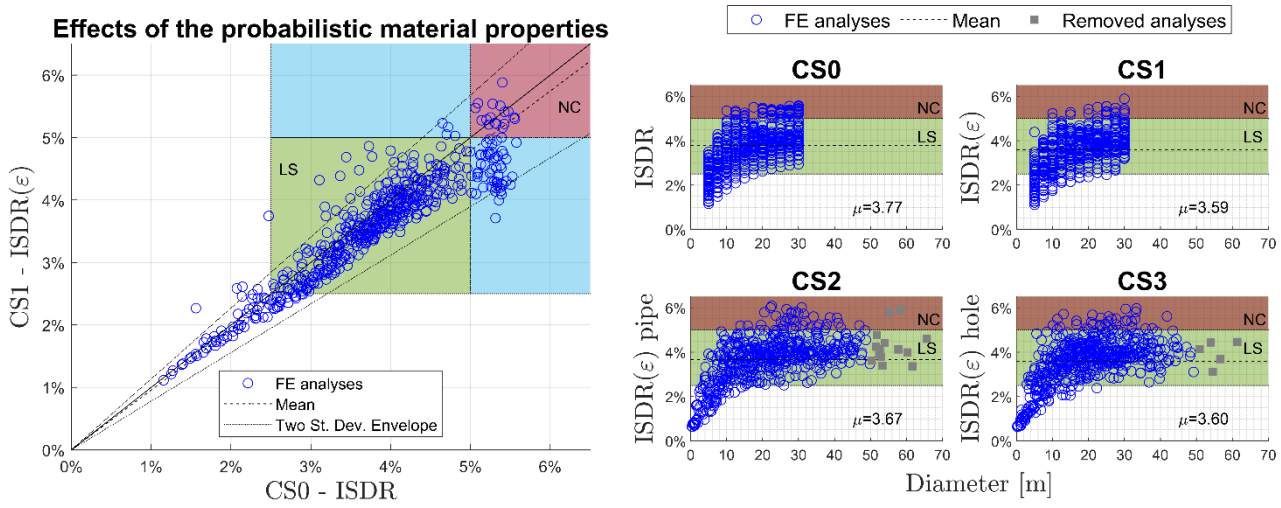

a) *b)*

Figure 5. Influence on the ISDR: a) of the uncertainties in the material properties; b) of the uncertainties in the material properties and the diameter distribution

Finally, as shown in Figure 6, the near collapse limit state threshold (5%) was exceeded more frequently in CS0, whilst the 2.5% threshold exceedance occurred for all four case studies in a comparable number of analyses for a given fuel or structure-fire distance. Again, the trend of the results indicates that higher ISDR may be reached for the same fire scenario when the deterministic material properties are employed (CS0), for which plasticity and load redistribution occur for lower load levels or fire intensity compared to the case studies with the probabilistic material model (CS1-CS3).

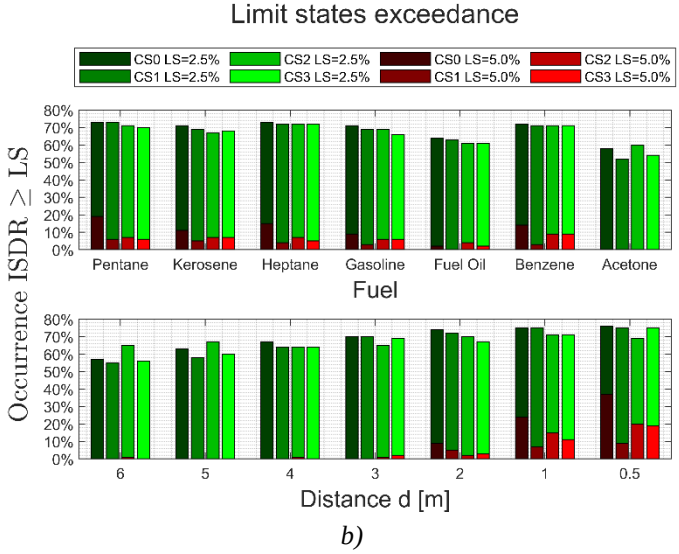

b)

Figure 6. a) LS thresholds exceedance for type of fuel and for distance d

3.4. Cloud analysis and Multiple stripe analysis

Though numerous probabilistic seismic demand models (PSDM) are available, the literature is currently lacking extensive applications in the fire context and only few probabilistic fire demand models (PFDM) can be found [21-25]. With respect to PSDM, incremental dynamic analysis (IDA), Cloud analysis (CA) and Multiple stripe analysis (MSA) are usually employed to obtain fragility curves. PSDMs are obtained with IDA by incrementing an IM in dynamic analyses until the EDP exceeds a certain limit state (LS). However, scaling fire IMs, such as fire load or heat flux, can rapidly lead to unrealistic fire scenarios and thus, IDA is not well suited for a PFDM and is not applied in this work. Instead, both CA, also employed in [43] and MSA are proposed to develop the PFDM.

3.4.1. Cloud Analysis (CA)

Cloud analysis (CA) is suited to build a PSDM from EDP-IM pairs arranged in a data cloud. This procedure is particularly convenient as it does not require to perform several analyses for discrete quantities of IM as in MSA and thus, it is not necessary to determine the IM to be employed in the PSDM model a priori. This allows for the selection of the most suitable IM a posteriori, i.e., in light of the results of the numerical analyses and of the CA.

The CA method assumes that an EDP follows a lognormal distribution when conditioned on an IM. Hence, the probabilistic demand model can be characterised as follows

$$\widehat{\mathrm{EDP}} = a\mathrm{IM}^{b}$$
$$\ln\left(\widehat{\mathrm{EDP}}\right) = A + B\ln(\mathrm{IM}) \tag{9}$$

where $\widehat{\mathrm{EDP}}$ is the median of the EDP, and the parameters $a = \exp(A)$ and $b = B$ are identified by means of a linear regression. Indeed, the conditional median of the EDP given the IM is linear in the log–log space, whereas the conditional dispersion of the EDP given the IM is constant. Such dispersion, referred to as $\beta_{\mathrm{EDP|IM}}$, can be determined as the standard deviation of the linear regression $\sigma_{ln(\mathrm{EDP})|\mathrm{IM}}$

$$\beta_{\mathrm{EDP|IM}} = \sigma_{ln(\mathrm{EDP})|\mathrm{IM}} = \sqrt{\frac{\sum_{\mathrm{i}=1}^{n}\left[\ln(\mathrm{EDP_i}) - \ln\left(\widehat{\mathrm{EDP_i}}\right)\right]^2}{n-2}} \quad (10)$$

Finally, the fragility function can be defined in the form of a lognormal cumulative distribution function [42]

$$\mathrm{P(EDP > LS|IM)} = 1 - \Phi\left(\frac{\ln\left(\frac{\mathrm{LS}}{a\mathrm{IM}^b}\right)}{\beta_{\mathrm{EDP|IM}}}\right) \quad (11)$$

3.4.2. Multi Stripe Analysis (MSA)

MSA can be applied to build a demand model by considering a discrete set of IMs, so that EDP-IM pairs are arranged in a stripe for each IM level. However, a minimum number of analyses should be performed for each level of IMs to obtain meaningful models [15]. In the framework of this work, MSA analysis was employed for IMs and CSs that allowed for stripes with at least 7 occurrences, i.e., at least 7 analyses were performed for each value of the IM. Though at least 10 instances per stripe are usually suggested [15], the threshold was lowered to 7 to test the ability of MSA to provide efficient PFDMs with only few results for each IM level.

MSA is based on the definition of fraction of collapses for a predefined LS and for each i-th level of IM, i.e., for each stripe. Such fraction is obtained dividing the number k_I of analyses in which EDP > LS by the total number of analyses performed. Assuming that observations of "collapse" or "no-collapse" are independent for the different fire scenarios, a binomial distribution can be used to express the probability of observing k_I collapses among n_I fire scenarios given an IM_i

$$\mathrm{P}(k_i \text{ collapses in } n_i \text{ fire scenarios}) = \binom{n_i}{k_i} p_i^{k_i} (1-p_i)^{n_i - k_i} \quad (12)$$

where p_I is the probability to observe a collapse C given an IM_i. Such probability can be defined with a lognormal cumulative distribution function [18]

$$p_i = P_i(C|IM_i) = \Phi\left(\frac{\ln\left(\frac{IM_i}{\theta}\right)}{\beta}\right) \quad (13)$$

The function $\Phi(\ \ )$ is the standard normal cumulative distribution function, while θ and β define the shape of the fragility function and are the median of the fragility function, i.e., the IM level generating a probability of exceedance of 50%, and the standard deviation of $\ln(\mathrm{IM})$, respectively. The parameter β is the dispersion of the fragility function and must not be confused with the term $\beta_{\mathrm{EDP|IM}}$ in Eq. (10), which is the dispersion of the EDP conditioned on IM. In this work the fragility function is built with the maximum likelihood method, which aims at finding the probability distribution with the highest likelihood of having produced the fraction of collapse observed for each $\mathrm{IM_i}$. The likelihood is defined as the product of the binomial probabilities

$$\begin{aligned}&\mathrm{Likelihood} = \prod_{i=1}^{m} \binom{\mathrm{n_i}}{\mathrm{k_i}}\ \mathrm{p_i^{k_i}}\ (1-\mathrm{p_i})^{\mathrm{n_i}-\mathrm{k_i}}\\ &\mathrm{Likelihood} = \prod_{i=1}^{m} \binom{\mathrm{n_i}}{\mathrm{k_i}}\ \Phi\left(\frac{\ln\left(\frac{\mathrm{IM_i}}{\theta}\right)}{\beta}\right)^{\mathrm{k_i}} \left(1-\Phi\left(\frac{\ln\left(\frac{\mathrm{IM_i}}{\theta}\right)}{\beta}\right)\right)^{\mathrm{n_i}-\mathrm{k_i}}\end{aligned} \tag{14}$$

where m is the number of IM levels or stripes. The optimal parameters $\hat{\theta}$ and $\hat{\beta}$ of the fragility function are obtained by maximising the likelihood as follows

$$\{\hat{\theta},\hat{\beta}\} = \max_{\theta,\beta} \sum_{\mathrm{i=1}}^{\mathrm{m}} \left[\ln\binom{\mathrm{n_i}}{\mathrm{k_i}} + \mathrm{k_i}\ln\Phi\left(\frac{\ln\left(\frac{\mathrm{IM_i}}{\theta}\right)}{\beta}\right) + (\mathrm{n_i}-\mathrm{k_i})\ln\left(1-\Phi\left(\frac{\ln\left(\frac{\mathrm{IM_i}}{\theta}\right)}{\beta}\right)\right)\right] \tag{15}$$

Once the optimal parameters are defined, the fragility function can be obtained employing the distribution assumed earlier (Eq.(13))

$$\mathrm{P(EDP} > \mathrm{LS|IM)} = \Phi\left(\frac{\ln\left(\frac{\mathrm{IM}}{\hat{\theta}}\right)}{\hat{\beta}}\right) \tag{16}$$

The dispersion of the EDP conditioned on the IM for the i-th stripe $\beta_{\mathrm{EDP}_i|\mathrm{IM}_i}$ can be taken as in [25].

$$\begin{aligned}&\beta_{\mathrm{EDP}_i|\mathrm{IM}_i} = \frac{\sigma_{\mathrm{EDP}_i|\mathrm{IM}_i}}{\mu_{\mathrm{EDP}_i|\mathrm{IM}_i}}\\ &\sigma_{\mathrm{EDP_i|IM_i}} = \sqrt{\frac{\sum_{\mathrm{i=1}}^{\mathrm{o}}\left[\mathrm{EDP_{i,o}}-\mu_{\mathrm{EDP_i|IM_i}}\right]^2}{n}} \quad \mu_{\mathrm{EDP}_i|\mathrm{IM}_i} = \frac{\sum_{\mathrm{i=1}}^{o}\mathrm{EDP_{I,o}}}{n} \quad \text{with o=occurrences at } \mathrm{IM_i}\end{aligned} \tag{17}$$

3.5.CA and MSA results

In order to derive the fire fragility curves, the results of the four case studies were analysed by means of CA and MSA. The ISDR was used as unique EDP and the IMs given in Table 4 were exploited. The CA was applied to all cases and all IMs, as mentioned in Section 3.4, whilst the MSA was employed only when at least 7 instances per stripe were available. As a result, the MSA was applied to CS0 and CS1 for IMs consisting of single fire parameters or simple functions of them, i.e., D, d, q, L/D and L_f; while, due to the variability of the diameters D introduced in the analyses, MSA was used only for d and q in CS2 and CS3. Indeed, it appears that obtaining well-defined stripes is not trivial when uncertainties are included into the demand model as continuous probabilistic density functions. The obtained PFDMs are shown against the numerical results in an EDP-IM space in Figure 7. The CA regression is represented as a continuous line, while single points are used for each stripe of the MSA. A log-log space representation is preferred to better show the linear regression fit when only the CA is available. The parameters of the CA and the MSA defined in Sections 3.4.1 and 3.4.2 are reported in Table 5 and Table 6, respectively.

Table 5. Cloud analysis parameters

CA parameters								
IM	**CS0**		**CS1**		**CS2**		**CS3**	
	a	*b*	*a*	*b*	*a*	*b*	*a*	*b*
D	0.014	0.355	0.014	0.336	0.012	0.373	0.012	0.384
d	0.043	-0.188	0.040	-0.163	0.039	-0.138	0.039	-0.162
q	0.030	0.210	0.029	0.199	0.028	0.218	0.028	0.212
L/D	0.026	-0.975	0.025	-0.902	0.025	-0.912	0.026	-0.864
L_f	0.009	0.422	0.009	0.399	0.008	0.457	0.007	0.469
HFavg	0.007	0.620	0.007	0.569	0.005	0.706	0.005	0.708
d/L_f	0.020	-0.251	0.020	-0.227	0.017	-0.284	0.017	-0.289
$d/A_{b,PE,eq}$	0.018	-0.185	0.018	-0.170	0.017	-0.185	0.017	-0.186

Table 6. Multiple stripe analysis parameters

MSA parameters									
IM		**CS0**		**CS1**		**CS2**		**CS3**	
		$\hat{\theta}$	$\hat{\beta}$	$\hat{\theta}$	$\hat{\beta}$	$\hat{\theta}$	$\hat{\beta}$	$\hat{\theta}$	$\hat{\beta}$
Life safety limit state	D	5.911	0.461	6.209	0.550	-	-	-	-
	d	17.601	1.401	15.627	1.474	4748.121	6.707	26.229	2.125
	q	0.323	1.523	0.465	1.367	0.249	1.948	0.409	1.598

LS=2.5%	L/D	1.071	0.189	1.034	0.214	-	-	-	-
	L_f	12.046	0.319	12.882	0.338	-	-	-	-
Near collapse limit state	D	43.435	0.750	138.181	1.137	-	-	-	-
	d	0.500	0.923	0.107	1.496	0.248	1.227	0.254	1.143
	q	7.954	0.920	21.924	1.151	49.972	2.011	34.131	1.676
LS=5.0%	L/D	0.541	0.056	0.466	0.133	-	-	-	-
	L_f	58.685	0.489	121.218	0.719	-	-	-	-

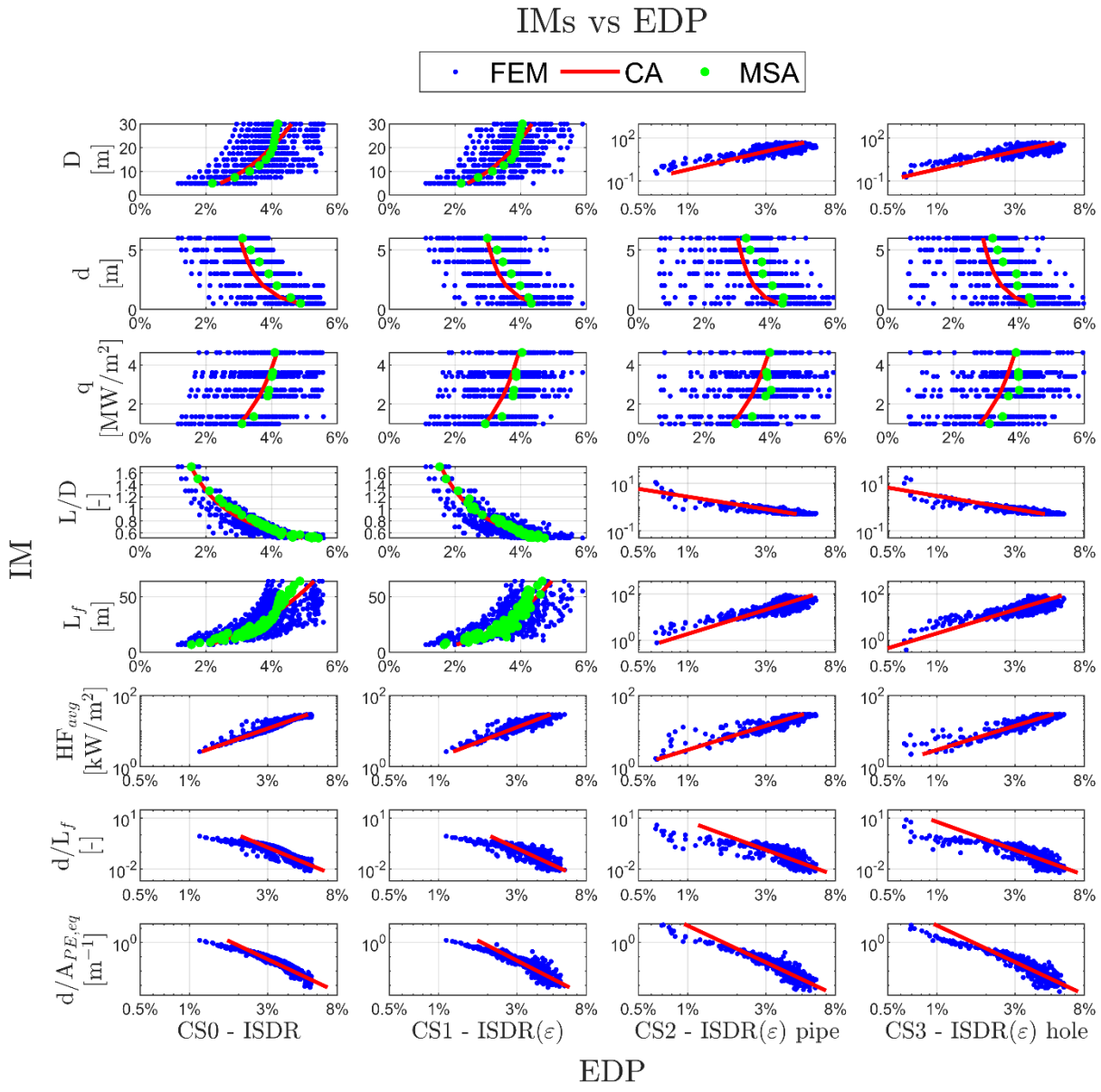

Figure 7. Cloud and multi-stripe analysis fit models

Not all IMs allow for equally well-defined PFDMs and the dispersion of the EDP conditioned on IM $\beta_{\mathrm{EDP|IM}}$ provides a quantitative measure of the variations between the actual and the predicted EDP values for a given IM. Such dispersions are summarised in Figure 8 for all the derived PFDMs. When the MSA was used, dispersion values were determined according to Eq. (17) at each IM level. As

expected, the MSA applied with L/D and L_f as IMs, showed the highest variability in the dispersion because only 7 analyses per stripe were used, confirming that at least 10 analyses for each IM level [15] are probably necessary to obtain efficient demand models.

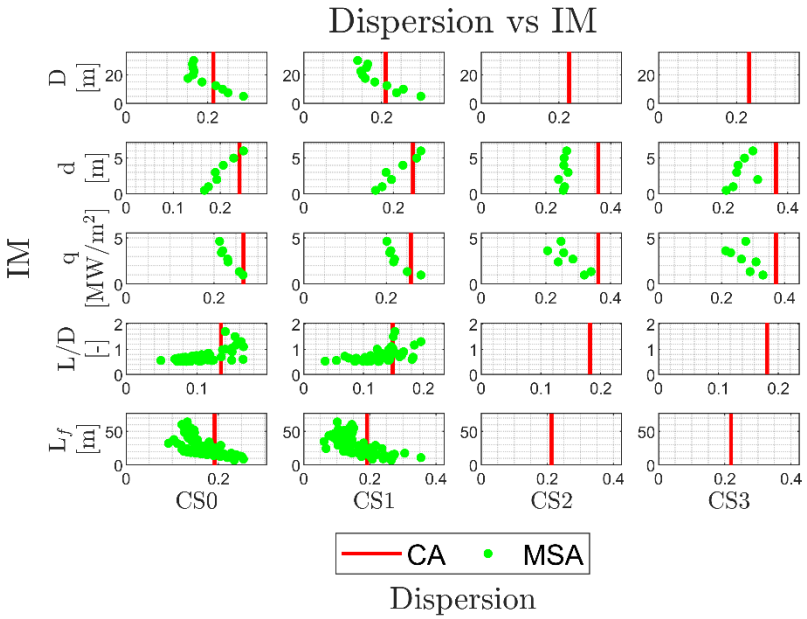

Figure 8. Cloud vs multi-stripe analysis dispersions

In fact, the dispersion is a good indicator to evaluate the efficiency of an IMs. An IM is efficient if it generates low $\beta_{\mathrm{EDP|IM}}$ values, usually below 0.3 [15]. Therefore, the dispersion of the CA was employed to select the best IM candidates for developing the fire fragility curves. Dispersions were compared in the efficiency plot of Figure 9a, from which it can be observed that for CS2 and CS3 q and d, which are the only IMs completely independent from the diameter D (Table 4), cannot be deemed efficient. This is due to the fact that the fire diameter D is a fundamental parameter to characterise the fire severity and this is even more true when a probabilistic distribution of D is assumed as in CS2 and CS3. Nevertheless, even though for CS0 and CS1 q and d can be considered efficient, they show the highest dispersion values among the different IM. Based on this discussion, q and d were discarded and among the remaining IM candidates, the three with the highest efficiency were selected, namely L/D, HF_{avg} and $d/A_{b,PE,eq}$.

Besides, the sufficiency of the IMs was investigated to ensure an accurate estimate of the probability of a structural response given an IM, i.e., P(EDP|IM). According to Luco and Cornell [19], IMs are sufficient when the structural response to a demand shows no trend in the correlation with the

parameters defining such demand. However, the IMs candidates employed in this work were defined as functions of the fire parameters, i.e., D, d and q, and correlation was always observed between the residuals of EDP and these parameters. In this situation, a more appropriate sufficiency measure is the relative sufficiency, which compares the sufficiency of IMs by evaluating the amount of information gained on average about the structural response. The amount of information *I* gained by IM_2 with respect to IM_1 can be evaluated according to [20]

$$\mathrm{I}(\mathrm{EDP}|\mathrm{IM}_2|\mathrm{IM}_1) \approx \frac{1}{\mathrm{n}}\sum_{\mathrm{i}=1}^{\mathrm{n}} \log_2 \frac{\mathrm{p}[\mathrm{EDP} = \mathrm{EDP}_\mathrm{i}|\mathrm{IM}_2]}{\mathrm{p}[\mathrm{EDP} = \mathrm{EDP}_\mathrm{i}|\mathrm{IM}_1]}$$

$$\mathrm{P}(\mathrm{EDP} = \mathrm{EDP}_\mathrm{i}|\mathrm{IM}) = \frac{1}{\beta_{\mathrm{EDP}|\mathrm{IM}}\mathrm{EDP}_\mathrm{i}}\Phi\left(\frac{\ln\left(\frac{\mathrm{EDP}_\mathrm{i}}{a\mathrm{IM}_\mathrm{i}^{b}}\right)}{\beta_{\mathrm{EDP}|\mathrm{IM}}}\right) \tag{18}$$

and is expressed in unit of bits of information. EDP_i is the parameter evaluating the structural response (ISDR) for each of the n fire scenarios, $\mathrm{P}(\mathrm{EDP}|\mathrm{IM})$ is the probability of a structural response given the IM and $\Phi(\,)$ is the standard gaussian probability density function. An IM is more sufficient than another if it provides more information on the structural response. It follows that IM_2 is more sufficient than IM_1 for positive values of $\mathrm{I}(\mathrm{EDP}|\mathrm{IM}_2|\mathrm{IM}_1)$. The higher the value of $\mathrm{I}(\mathrm{EDP}|\mathrm{IM}_\mathrm{i}|\mathrm{IM}_1)$, the more sufficient the IM_i is. A relative sufficiency plot is depicted in Figure 9b, by comparing the amount of information *I* of the candidates IMs with respect to the diameter (IM_1=D). The choice of the reference IM is arbitrary, since selecting a different IM the relative sufficiency plot translates vertically, but the difference between the values of *I* for each IM remain unchanged. The three best IMs in terms of relative sufficiency are the same as for the efficiency and thus, no further consideration was necessary to choose the IMs for developing the fragility curves. For all the four sets of analyses $\mathrm{d}/\mathrm{A}_{\mathrm{b,PE,eq}}$ permits for dispersions and amounts of information comparable with the ones obtained considering $\mathrm{HF}_{\mathrm{avg}}$ as IM. However, $\mathrm{d}/\mathrm{A}_{\mathrm{b,PE,eq}}$ has the advantage of being much more straightforward to calculate than $\mathrm{HF}_{\mathrm{avg}}$. As expected, Figure 9 shows that IMs are less efficient and less sufficient when uncertainties are introduced, but their ranking remains unchanged. Moreover,

being d and q completely independent from the diameter D, their relative sufficiency is significantly worse when probabilistic distributions of the diameter are used (CS2 and CS3) and the diameter provides more relevant information to characterise the fire severity, and in turn the structural response.

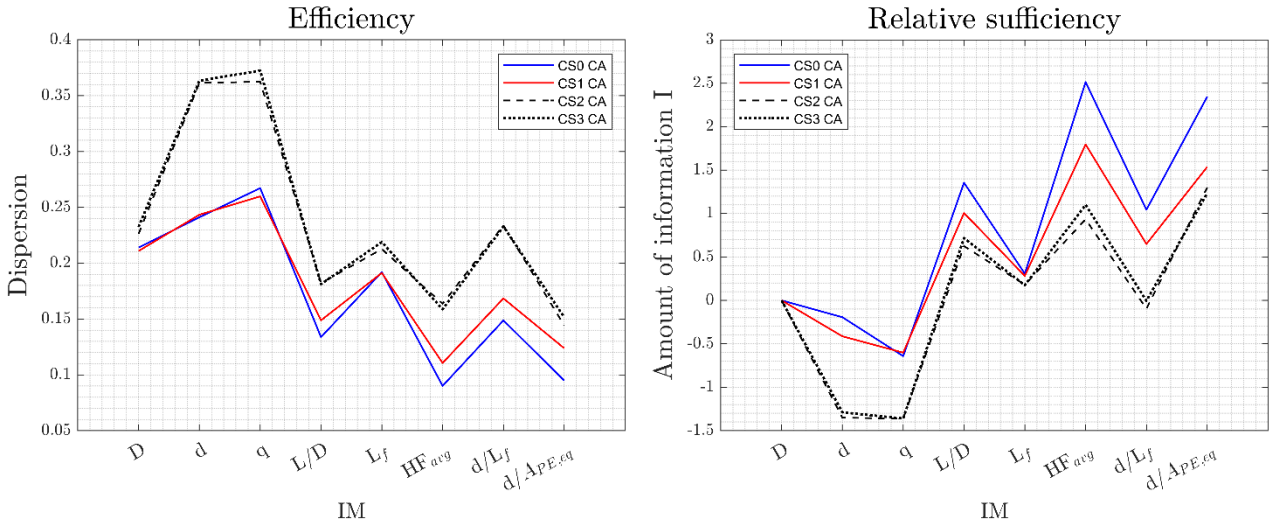

a) *b)*

Figure 9. a) Efficiency and b) relative sufficiency of IMs

3.6. Fire fragility curves

Fire fragility curves were derived from the PFDMs obtained for each of the IM candidates given in Table 4. However, only the fragility curves obtained for the three most efficient and sufficient IMs are shown and discussed. The proposed curves can be used to quantify the probability that a steel pipe-rack exposed to a localised fire exceeds a predetermined limit state. The curves are developed for two limit states, namely the near collapse limit state and life safety limit state, for which a 5% and a 2.5% threshold is set on the ISDR. Fragility curves were derived for all the case studies, i.e. CS0, CS1, CS2 and CS3.

Figure 10 shows the fragility curves for the PFDM based on L/D as IM. A limitation should be applied to this model since for L/D<0.5 part of the structure would be engulfed into the localised fire and a different structural response is expected, with the ISDR no longer being the most appropriate EDP. Therefore, these curves may not be suited for the range shaded in grey. All the fragility curves for a given limit state attain the median of the probability distribution, i.e., P(ISDR>LS|L/D)=50% at

similar ISDR values. For the life safety limit state the 50% probability is exceeded for 0.45<L/D<0.52, while for the near collapse limit state this occurs for 1.03<L/D<1.06. As expected, here and in all the subsequent figures, the fragility curves show a higher dispersion when the parameter uncertainties are incorporated, i.e. CS1, CS2, CS3.

For L/D fire fragility curves for CS0 and CS1 are obtained also from the MSA, as illustrated in Figure 10b. The fragility curves based on the MSA fit the fraction of collapses, intended as the ratio between the cases in which a limit state was exceeded over the total number of fire scenarios (539) given an IM_i. Though the IM ranges relevant to collapses are similar to the ones from CA, different values of probabilities of exceedance are found. For instance, a higher curve is derived for the near collapse in CS0, for which at L/D=0.5 the probability of exceedance is higher than 90%. Conversely, by comparing the CS1 case study at the near collapse limit state the MSA and the CA provide similar fragility curves. This was also observed at the life safety limit state for which good agreement between the two methods to derive fragility curves is shown in Figure 10. However, since only few data were available for each stripe (7 or 14) and the curve fit rather disperse fraction of collapses, the MSA based fragility curves are deemed less reliable and the use of CA is suggested when less than 10 data are available for each IM level, as recommended in [15].

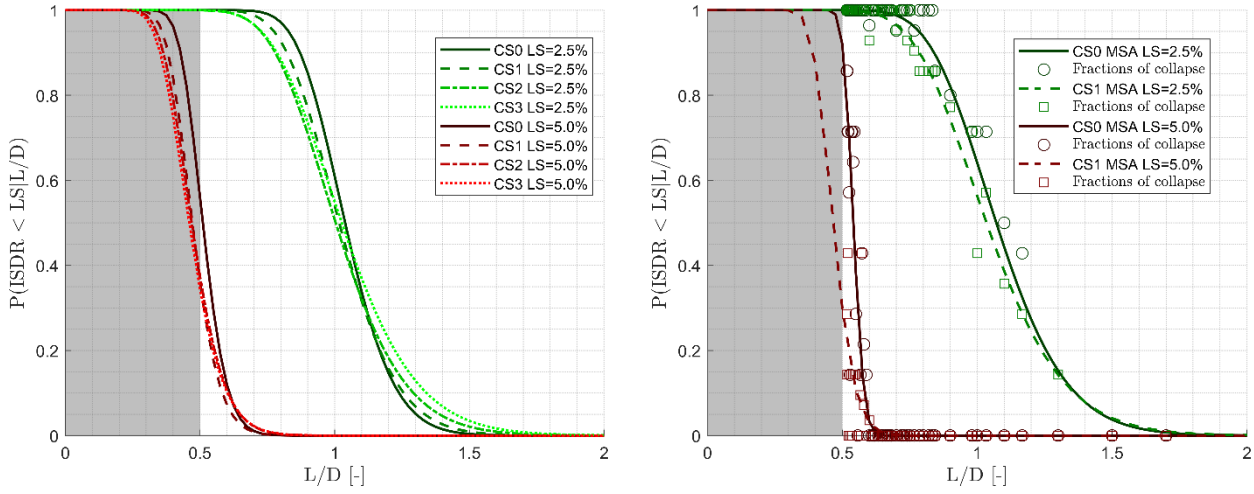

a) *b)*

Figure 10 fragility curves for near collapse and life safety preventions with L/D as IM. a) CA; b) MSA

A significant improvement in efficiency and relative sufficiency was obtained by employing HF_{avg} and $d/A_{b,PE,eq}$, whose associated CA based fragility curves are depicted in Figure 11a and Figure

11b, respectively. In Figure 11a, the probability of exceeding the life safety and the near collapse limit states surpasses the 50% for $8.7<HF_{avg}<10.8$ kW/m^2 and $26.6<HF_{avg}<31.1$ kW/m^2 respectively. For IM=$d/A_{b,PE,eq}$, the probability of exceeding the life safety and the near collapse limit states attains the 50% for $0.13<d/A_{b,PE,eq}<0.21$ m^{-1} and for $3.1\cdot10^{-3}<d/A_{b,PE,eq}<4.9\cdot10^{-3}$ m^{-1} respectively, as illustrated in Figure 11b.

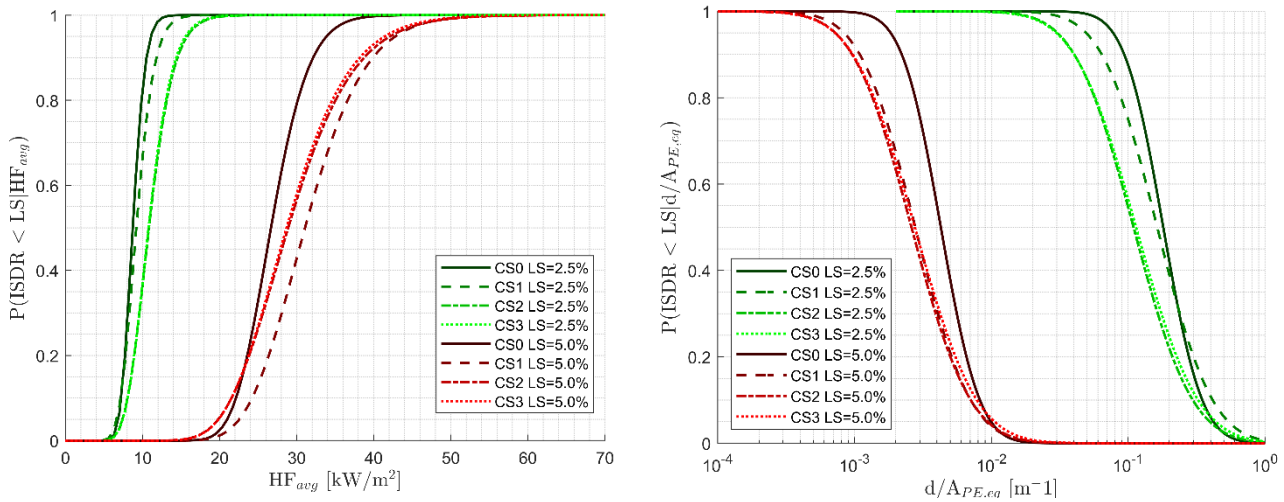

a) *b)*

Figure 11. CA based fragility curves for near collapse and life safety preventions with: a) HF_{avg} as IM; b) $\mathbf{d/A_{b,PE,eq}}$ as IM

It is interesting to note that in general, the fragility curves show lower probabilities of exceedance for a given value of IM when the probabilistic model for the steel strength at elevated temperature is considered (CS1-CS3 in Figure 10 and Figure 11). However, this may not be true for low probabilities of exceedance owing to the higher dispersions found in CS1 to CS3. This is a typical effect when considering parameter uncertainties, as the introduction of further uncertainties inflates the tails of the probability distributions, causing their cumulative distributions, i.e., the fragility functions, to span over larger IM ranges. Nevertheless, the medians of the probability distributions, i.e., the values of IM for which a probability of exceedance of 50% is reached, are always less demanding for CS1-CS3. Therefore, it can be concluded that in general less severe fragility curves are obtained when the probabilistic model for the steel strength is considered. This was expected because the retention factors at elevated temperature included in Eurocode are for design purposes and thus, inherently

conservative. Indeed, in the probabilistic model the retention factor k_y of the steel yield strength f_y in CS1 - CS3 is higher than the nominal one $k_{y,EN1993-1-2}$ used in CS0 (see Figure 3a).

In addition, the employment of probabilistic fire diameter distributions rather than a uniform one may have a significant influence on the fragility curves (CS1 vs CS2 and CS3), whilst very similar curves are always found for two normal diameter distributions with different mean and standard deviation because of the different type of leakage, i.e. CS2 vs CS3. Hence, the fragility curves seem more sensitive to the fact that a discrete diameter distribution is employed, rather than to the variation of the mean and standard deviation of the diameter of continuous density probability distributions. It should be noted that the difference in the mean and standard deviations of the normal distributions between leakage from a hole and from a pipe is in the order of about 12%. Moreover, it cannot be concluded that discrete diameter distributions always provide more severe fragility functions. Indeed, as shown in Figure 11, CS2 and CS3 fragility curves may be more or less severe than the ones from CS1 depending on the limit state and on the IM. Nevertheless, the definition of fire demand models based on probabilistic distributions is desirable and should be preferred since they provide more realistic fire scenarios based on leakage from a hole in the tank (CS2) or from a pipe (CS3).

4. Conclusions

The paper presented the development of probabilistic fire demand models for a prototype steel pipe-rack exposed to localised fires by adding uncertainties related to the structural capacity, i.e. yield strength, and to the fire diameter that is caused by a hole in a tank or by a hole in a pipe. PFDMs were defined for each case study by means of the Cloud analysis (CA) and, when suitable, also through the Multiple stripe analysis (MSA). It is shown that the CA is a viable method to derive PFDMs and fire fragility curves, whilst in order to benefit from the application of MSA, suitable IMs should be identified before performing the analyses so as to obtain stripes with at least 10 instances by scaling the severity of the fire based on such IMs. As expected, by allowing for the uncertainty of the steel yield strength, lower values of ISDR with respect to the reference case study CS0 were observed

because the retention factors, and in turn the yield strength values at elevated temperature were, on average, larger than the ones prescribed in EN 1993-1-2. Indeed, the steel structural members plasticized later with the probabilistic material model (CS1, CS2 and CS3), allowing for both a delay in load redistribution and smaller displacements, therefore resulting in less severe fragility curves. The fire fragility curves were derived for different EDP-IM candidates. In this respect, the most suitable IMs for steel pipe-racks, with similar characteristics with the prototype one, exposed to localised fires were identified as the ones that maximise the efficiency (lowest dispersion of the EDP given the IM) and the relative sufficiency (highest amount of information on the structural response). Three suitable IMs were identified: i) the fire position-diameter ratio L/D, which is easy to use for practitioners, but has lower efficiency and relative sufficiency indicators among the three proposed IMs; ii) the maximum average heat flux impinging the structure HF_{avg} and iii) the scaled distance $d/A_{b,PE,eq}$, which consists of a simple function of the fire parameters q, d and D, derived in similar fashion for explosion hazard as the structure-explosion distance over a fractional power of an equivalent TNT mass. The HF_{avg} and the $d/A_{b,PE,eq}$ are more efficient and more relatively sufficient IMs, but the maximum average heat flux impinging the structure HF_{avg} is not as straightforward to calculate as the scaled distance $d/A_{b,PE,eq}$, that showed comparable efficiency and sufficiency with HF_{avg} and accounts for the effects of the distance of the fire from the structure and the extension of the fire. MSA based fragility curves with L/D as IM were developed for the CS0 and CS1, but only 7 analyses were available for some stripes and thus, the CA fragility functions are deemed more reliable. Furthermore, probabilistic diameter distributions in CS2 and CS3 had influence on the fragility curves by lowering the probability of exceedance of the limit states for same values of IM and should be considered since they provide more realistic fire scenarios. In general, the definition of fire demand models based on probabilistic distributions for demand and capacity is desirable and should be preferred since they provide more realistic fire scenarios. Future perspectives will focus on considering multiple burning pool fires and the presence of the wind.

Acknowledgements

This research has been funded by the European XP-Resilience project through the grant agreement number 721816. The support received from the Italian Ministry of Education, University and Research (MIUR) in the frame of the 'Departments of Excellence' (grant L 232/2016) is gratefully acknowledged.

Compliance with Ethical Standards

I. Ethical approval

No human participants or animals were involved in the research.

II. Funding details (In case of Funding)

Ministero dell'Istruzione, dell'Università e della Ricerca; Grant: L 232/2016

Horizon 2020 Framework Programme; Award number: 721816; Recipient: Jerome Randaxhe

III. Conflict of interest

The authors declare that there are no conflicts of interest

IV. Informed Consent

No human participants or animals were involved in the research.

References

1. European Comitee for Standardisation (2002). Eurocode 1 Actions on structures – Part 1–2: General actions – actions on structures exposed to fire.
2. Franssen JM, Gernay T. Modeling structures in fire with SAFIR®: theoretical background and capabilities. J Struct Fire Eng 2017;8(3):300–23.
3. Bailey, C. G. 1998. "Development of computer software to simulate the structure behaviour of steel-framed buildings in fire." Comput. Struct. 67 (6): 421–438. https://doi.org/10.1016/S0045-7949(98)00096-0.
4. ABAQUS. 2014a. ABAQUS version 6.14, User's manual. Vélizy-Villacoublay, France: Dassault Systèmes.
5. ANSYS Inc. 2016. ANSYS versrefboion 17.0, User's manual. Canonsburg, PA: ANSYS.

6. DIANA FEA BV. 2016. DIANA version 10.1, User's manual. Delft, Netherlands: DIANA FEA BV.
7. Possidente L., Tondini N., Battini J.-M. (2019). Branch-switching procedure for post-buckling analyses of thin-walled steel members in fire. Thin-Walled Structures 136, 90-98.
8. Possidente L., Tondini N., Battini J.-M. (2020). 3D Beam Element for the Analysis of Torsional Problems of Steel-Structures in Fire. J. Struct. Eng., 146:(7), 10.1061/(ASCE)ST.1943-541X.0002665.
9. Rackauskaite, E., Kotsovinos, P., Rein, G. (2017). Structural response of a steel-frame building to horizontal and vertical travelling fires in multiple floors. Fire Saf. J. 91, 542–552. http://dx.doi.org/10.1016/j.firesaf.2017.04.018
10. Gernay, T., Khorasani, N.E. (2020). Recommendations for performance-based fire design of composite steel buildings using computational analysis. J. Constr. Steel Res. 166. https://doi.org/10.1016/j.jcsr.2019.105906
11. Possidente L., Tondini N., Battini J.-M. (2020). Torsional and flexural-torsional buckling of compressed steel members in fire. Journal of Constructional Steel Research: 171
12. Bergmeister, K., Brunello, P., Pachera, M., Pesavento, F., Schrefler, B.A. (2020). Simulation of fire and structural response in the Brenner Base Tunnel by means of a combined approach: A case study. Eng. Struct. 211. https://doi.org/10.1016/j.engstruct.2020.110319
13. Possidente L., Weiss A., de Silva D., Pustorino S., Nigro E., Tondini N. (2021) Fire safety engineering principles applied to a multi-storey steel building, Proceedings of the Institution of Civil Engineers - Structures and Buildings, 174(9), pp. 725-738, https://doi.org/10.1680/jstbu.20.00110
14. Bilotta A., de Silva D., Nigro E. (2016) General approach for the assessment of the fire vulnerability of existing steel and composite steel concrete structures, Journal of Building Engineering: 8, 198-207.
15. Mackie KR, Stojadinovic B. (2005) Comparison of incremental dynamic, cloud, and stripe methods for computing probabilistic seismic demand models. In: Structures congress. https://doi.org/10.1061/40753(171)184
16. Shome N, Cornell CA, Bazzurro P, Carballo JE. (1998) Earthquakes, records, and nonlinear responses. Earthq Spectra;14:469–500.

17. Cornell CA, Jalayer F, Hamburger RO, Foutch DA (2002). Probabilistic basis for 2000 SAC federal emergency management agency steel moment frame guidelines. J Struct Eng: 526–33.
18. Baker JW. (2015) Efficient analytical fragility function fitting using dynamic structural analysis. Earthq Spectra;31:579–99.
19. Luco N, Cornell CA. (2007) Structure-specific scalar intensity measures for near-source and ordinary earthquake ground motions. Earthq Spectra;23(2):357–92.
20. Ebrahimian H, Jalayer F, Lucchini A, Mollaioli F, Manfredi G. (2015) Preliminary ranking of alternative scalar and vector intensity measures of ground shaking. Bull Earthq Eng:2805–40.
21. Nigro, E., Bilotta, A., Asprone, D., Jalaver, F., Prota, A., Manfredi, G., (2014). Probabilistic approach for failure assessment of steel structures in fire by means of plastic limit analysis. Fire Saf. J. 68, 16–29.
22. Gernay T, Khorasani NE, Garlock M.(2016) Fire fragility curves for steel buildings in a community context: a methodology. Eng Struct;113:259–76.
23. Gernay T, Khorasani NE, Garlock M. (2019) Fire fragility functions for steel frame buildings: sensitivity analysis and reliability framework. Fire Technol;55(4): 1175–210.
24. Lange D, Devaney S, Usmani A. (2014) An application of the PEER performance based earthquake engineering framework to structures in fire. Eng Struct;66: 100–15.
25. Shrivastava M, Abu AK, Dhakal RP, Moss PJ. (2019) Severity measures and stripe analysis for probabilistic structural fire engineering. Fire Technol;55(4):1147–73.
26. Cornell CA, Krawinkler H. (2003) Progress and challenges in seismic performance assessment. Peer Cent News;3(2):1–3
27. Campedel M. (2008) Analysis of major industrial accidents triggered by natural events reported in the principal available chemical accident databases. University of Bologna, European Commission Joint Research Centre Institute for the Protection and Security of the Citizen.
28. Paolacci F. (2010) Structural safety of industrial steel tanks; pressure vessels and piping – basic seismic structural design of a typical piping system. University of RomaTre.

679 29. Bursi O, Paolacci F, Reza MS, Alessandri S, Tondini N. (2010) Seismic assessment of petrochemical
680 piping systems using a performance-based approach. J Press Vessel Technol.
681 30. Paolacci F, Bursi O, Reza MdS, Kumar A, Gresnigt AM. (2013) Main issues on the seismic design of
682 industrial piping systems and components. In: ASME 2013 pressure vessels & piping division
683 conference; p. 1–10.
684 31. Bursi O, Paolacci F, Reza MS. (2015) Performance-based analysis of coupled support structures and
685 piping systems. In: ASME 2015 pressure vessels & piping division conference; no. July.
686 32. Bernier C, Padgett JE. (2019) Fragility and risk assessment of aboveground storage tanks subjected to
687 concurrent surge, wave, and wind loads. Reliab Eng Syst Saf no.February.
688 33. Uehara V. (1991) Fire safety assessments in petrochemical plants. In: Fire safety science – third
689 international symposium; p. 83–96.
690 34. Chang JI, Lin C. (2005) A study of storage tank accidents. J Loss Prev Process Ind;19:51–9.
691 35. Zheng B, Chen G. (2011) Storage tank fire accidents. Process Saf Prog;30(3).
692 36. Shu C, Chong C. (2009) Applications of 3D QRA technique to the fire/explosion simulation and
693 hazard mitigation within a naphtha-cracking plant. J Loss Prev Process Ind;22(4):506–15.
694 37. Committee for the prevention of disasters by hazardous materials (2005) Methods for the calculation
695 of physical effects due to releases of hazardous materials – Yellow Book. Gevaarlijke Stoffen, The
696 Hague.
697 38. Vílchez JA, Espejo V, Casal J. (2011) Generic event trees and probabilities for the release of different
698 types of hazardous materials. J Loss Prev Process Ind;24(3):281–7.
699 39. Moosemiller M. (2011) Development of algorithms for predicting ignition probabilities and explosion
700 frequencies. J Loss Prev Process Ind;24(3):259–65.
701 40. Gottuk DT, White DA. (2016) Liquid fuel fires. SFPE Handb Fire Prot Eng;12:2552–90.
702 41. Elhami Khorasani N, Gardoni P, Garlock M. (2015) Probabilistic fire analysis: material models and
703 evaluation of steel structural members. J Struct Eng ASCE 141(12)
704 42. Qureshi R, Ni S, Elhami Khorasani N, Van Coile R; Hopkin, Gernay T (2020) Probabilistic Models
705 for Temperature-Dependent Strength of Steel and Concrete. J Struct Eng ASCE 146(6)

706 43. Randaxhe J, Popa N, Tondini N (2021) Probabilistic fire demand model for steel pipe-racks exposed
707 to localised fires. Engineering Structures 226
708 44. Thomas PH. (1963) The size of flames form natural fires. In: Symposium international on combustion,
709 vol. 9. p. 844–59.
710 45. Mudan KS. (1984) Thermal radiation hazards from hydrocarbon pool fires. Prog Energy Combust
711 Sci;10:59–80.
712 46. Heskestad G. (1984) Engineering relations for fire plumes. Fire Saf J;7(2):25–32.
713 47. Rew PJ, Hulbert WG. (1996) Development of pool fire thermal radiation model. In: HSE Contract
714 Research Report.
715 48. Babrauskas V. (1983) Estimating large pool fire burning rates. Fire Technol:251–61.
716 49. Shokri M, Beyler CL. (1989) Radiation from large pool fires. SFPE J Fire Protect Eng; 4(1):141–50.
717 50. Society of Fire Protection Engineers (2016) SFPE handbook of fire protection engineering. 6th ed.
718 US: Springer.
719 51. Kamikawa D, Hasemi Y, Wakamatsu T, Kagiya K. (2003) Experimental flame heat transfer
720 correlations for a steel column adjacent to and surrounded by a pool fire. Fire Saf Sci - Seventh Int
721 Symp:989–1000. https://doi.org/10.3801/IAFSS.FSS.7-989.
722 52. Hanus F, Vassart O, Tondini N, Nadjai A, Franssen J. (2016) Temperature assessment of a vertical
723 steel member subjected to localised fire: experimental tests. In: Proceedings of the 9th conference on
724 structures in fire.
725 53. Tondini N, Franssen J-M. (2017) Analysis of experimental hydrocarbon localised fires with and
726 without engulfed steel members. Fire Saf J;92(May):9–22.
727 54. Francis P, Baddo N, Hanus F, Thauvoye C. (2018) Design of columns subject to localised fires. The
728 Steel Construction Institute (SCI).
729 55. Tondini N, Thauvoye C, Hanus F, Vassart O. (2019) Development of an analytical model to predict
730 the radiative heat flux to a vertical element due to a localised fire. Fire Saf J;105(March):227–43.
731 56. Yamaguchi T., Wakasa K. (1986). Oil pool fire experiment. In: Fire Safety Science – First
732 international symposium. pp. 911–18.

57. European Comitee for Standardisation (2005). Eurocode 3 Design of steel structures - Part 1-2: General rules - Structural fire design.
58. Zabetakis MG, Burgess DS. (1960). Research on the hazards associated with the production and handling of liquid hydrogen, Ohio, USA.
59. Drysdale D. (2011) An introduction to fire dynamics. 3rd ed. John Wiley & Sons.
60. Van Coile R., Elhami Khorasani N., Lange D., Hopkin D. (2021) Uncertainty in Structural Fire Engineering, International Handbook of Structural Fire Engineering, pp 323–411
61. Singh. K., Gardoni P., Stochino F. (2020). Probabilistic models for blast parameters and fragility estimates of steel columns subject to blast loads, Engineering Structures;222
62. Song X. (2020). Parameterized fragility analysis of steel frame structure subjected to blast loads using Bayesian logistic regression method, Structural Safety; 87
63. Zhang C., Gholipour G., Mousavi A. A. (2019). Nonlinear dynamic behavior of simply-supported RC beams subjected tocombined impact-blast loading. Engineering Structures;181:124-142
64. FEMA and ASCE, (2000) FEMA 356 – Prestandard and commentary for the seismic rehabilitation of buildings, no. November. Federal Emergency Management Agency.
65. Phan H, Paolacci F, Corritore D, Tondini N, Bursi O, (2019) A Kriging-Based Surrogate Model for Seismic Fragility Analysis of Unanchored Storage Tanks, ASME 2019 Pressure Vessels & Piping Conference